Iran Polym J (2013) 22:519–536
DOI 10.1007/s13726-013-0152-4

ORIGINAL PAPER

TG/FTIR/MS study on the influence of nanoparticles content upon the thermal decomposition of starch/poly(vinyl alcohol) montmorillonite nanocomposites

Manuela-Tatiana Nistor · Cornelia Vasile

Received: 9 October 2012 / Accepted: 21 April 2013 / Published online: 30 April 2013

Abstract The effect of the nanoclay content on the thermal decomposition of nanocomposites based on poly(vinyl alcohol)/thermoplastic starch, as intercalated hybrids, has been established. The changes in the decomposition products distribution and their evolution have been investigated by coupled thermogravimetric analysis, Fourier transform infrared spectroscopy, and mass spectrometry. Detailed analysis of the in situ vapor phase showed that the poly(vinyl alcohol)/starch/clay nanocomposites display a completely different distribution pattern of degradation product, depending on nanoclay content. By in situ vapor phase FTIR and MS spectroscopic techniques, both decomposition compounds of the constituent polymers and some new ones, depending on the nanoparticles content, are identified. The effect of the increase in nanoparticles content consists mainly in variation of some volatile compounds evolution, such as formic acid, water, formaldehyde, propionic acid, methanol, acetic acid carbon dioxide, benzene, etc., which in the case of nanocomposites is very complex. Thus, a content of 2–4 wt% organically-modified montmorillonite hinders the decomposition of the poly(vinyl alcohol)/starch blend. Both characteristic temperature of evolution of the main compounds increases by increasing its content and evolution starting time is delayed; while the untreated nanoclay acts like a catalyst, which decreases characteristic temperatures and evolution time with increasing its content. The temperature dependence of the maximum evolution rate of various compounds on the nanoclay content is very complex as, in the case of nanocomposites, of both primary and secondary reactions and transport phenomena occur simultaneously. Generally, this behavior is related to the dispersion of nanoclays in the polymeric matrix.

Keywords Polymer matrix composites · Thermal analysis · Nanocomposites · Poly(vinyl alcohol) · Starch · Nanoclay

Introduction

The layered silicate materials used as nanoscale reinforcements represent a very interesting topic in the research and applications of polymeric materials. As generally known, incorporation of 1–5 wt% montmorillonite content into a polymer matrix significantly improves its mechanical resistance, due to the nanometric dimensions of the clay nanoparticles and high aspect ratio. Nanoscale phase distribution as well as the polymer-layered silicate synergism confers additional properties, such as flame retardation, enhanced barrier properties, and ablation resistance.

Thermal stability is one of the most important characteristics of nanocomposites. In particular, thermal stability, depending on their structure and morphology, was considered as an important factor in nanocomposites applications [1]. Generally, if processing temperature is higher than the thermal stability of the organic component used for montmorillonite modification, decomposition will take place, leading to variations in material's structure. All polymer/clay nanocomposites preparations require high temperatures for their fabrication, while most polymeric materials require prolonged service in air at high temperatures. Thus, determination of the onset temperature for thermal degradation, of the resulting products of thermal degradation and stability of polymer in the presence of

M.-T. Nistor · C. Vasile (✉)
Department of Physical Chemistry of Polymers, "Petru Poni" Institute of Macromolecular Chemistry, 700487 Iasi, Romania
e-mail: cvasile@icmpp.ro

layered silicates, as well as understanding of the interrelationship between molecular structure, morphology and thermal stability (decomposition temperature, rate, and degradation products) of nanocomposites are critical [2, 3].

The relation between the degree of clay dispersion in the polymer matrix and the thermal stability of nanocomposite materials has been discussed in many studies [4–6]. Generally, if a higher degree of exfoliation is achieved, a stronger enhancement of thermal resistance could be expected. The degree of exfoliation is found to depend on montmorillonite concentration and it determines the changes in thermal stability. The maximum enhancement of thermal stability was observed for nanocomposites with lower filler content (1–2 wt%) in which homogeneous exfoliation and random dispersion of nanoparticles were maintained. The degree of intercalation/exfoliation and distribution of the silicate layers was found to change with the degree of nanofiller loading. Exfoliation was more likely to occur at a lower clay content (about 1 wt%), and an intercalated structure was basically observed for nanocomposites with a higher clay content. The increasing number of dispersed montmorillonite layers per volume unit of polymer matrix causes clay particles' arrangement in a more regular structure. In their study on thermal properties of epoxy/montmorillonite hybrid materials, Guo et al. [7] have emphasized that montmorillonite dispersion is crucial for the thermal stability of nanocomposites, as actually confirmed in other studies [8–10]. Dispersion was influenced by the nanofiller content, and thermal stability changes were observed with increasing clay loading. When the organo-modified montmorillonite (OMMT) loading degree was lower than 8 phr, the samples exhibited a higher thermal stability than those with a higher OMMT loading. When the OMMT loading further increased, the nanocomposites developed an intercalated structure. As a matter of fact, the number of exfoliated silicate platelets which are considered to be more effective in blocking heat and oxygen than tactoids decreases with the OMMT loading. Montmorillonites have been applied in polymers for many years [11, 12].

PVA/starch films can be used as bioartificial materials, chemically-bonded composites, and also as recyclable sizing agents; while foamed blends can be employed as disposable plates, cups, devices for transportation of powdery materials, as biodegradable packaging materials [13], etc. All these substances have received considerable attention in the last decades [14–16].

Less is known about the thermal behavior of nanocomposites containing both polymers—starch and poly (vinyl alcohol) [17].

In our previous paper [18], the effect of clay type on the decomposition pathway of nanocomposites' nature and composition of the decomposition products was studied. New products in gaseous and condensed phase have been identified, as additional degradation pathways were developed in the presence of nanoclays. The chemical species, trapped between MMT layers, have better chance to undergo further intermolecular reactions, such as radical recombination.

In this study, we intend to establish the effect of Nanocor I28 and Peruvian clay concentration on the thermal decomposition of poly(vinyl alcohol) (PVA)/starch nanocomposites as, at a 2 % incorporated content, these nanoclays showed very different actions; thus, the former improves thermal stability, while the latter acts as a catalyst, lowering the thermal properties. The behavior of the PVA/starch blend and of its nanocomposites with content of 1–5 wt% nanoclay has been investigated by thermogravimetric analysis coupled with FTIR and MS.

Experimental

Materials

AMYZ 100-type corn starch (S) (AMYLUM, Romania) with an acidity of 2.2 mg KOH/100 g sample, pH 4.9, 13.1 % humidity, 70 °C vitreous transition, and a crystallinity degree of 32 % (determined by XRD) was used for nanocomposites preparation.

Water-soluble poly(vinyl alcohol) (PVA) (Du Pont Comp.) is known under the trade name Elvaloy. The polymeric material has a residual poly(vinyl acetate) content of 0.5–1.8 %, hydrolysis degree: 99 mol %, viscosity: 27–38 mPa s, specific heat: 1674 J/kg K, glass transition temperature: 82 °C, and crystallinity degree: 30.6 %.

PVA/starch/clay-based nanocomposites have been obtained by extrusion compounding. A blend film with a 50-wt% PVA/50 wt% starch (PVA/TPS) composition was obtained by baking a mixture of granular starch (corn starch) and PVA and mixing it with a Brabender plastograph (Brabender® Elektromaschinen GmbH, Germany), followed by calendering and extrusion [19–21]. Blend conditioning by mechanical stirring was done before processing. The temperature profile zones of the 1/2/3/die (°C) were of 145/145/140/140, torque (N m) = 50–60, and screw speed sheet extrusion was of 30 rpm. The nanofillers used, such as Nanocor I28 and Peruvian clay produced by Nanocor, were montmorillonites.

Nanocor I28 (I28) is a layered silicate modified with trimethyldodecadecyl-ammonium ions. It has a non-homogeneous structure, because its galleries do not have the same size. It has the following formula: $Na_x[Al_{4-x}Mg_x](Si_8)O_{20}(OH)_4$, where $x = 0.7$–1.2, and aspect ratio ≈ 200. Peruvian clay (MMT) is an untreated montmorillonite.

The nanocomposites have been prepared starting from a 50-wt% PVA/50 wt% starch containing small amounts of plasticizer, such as glycerol, diethylene glycol, and entanglement compatibilizer, such as urea, which were used as received. Stabilizers, destructuring agents, additives for PVA and starch processing, and minimum percentage of water necessary for processing were also employed. For a 100-wt% blend, various montmorillonite silicate nanoparticles have been incorporated, in concentrations varying from 1 to 5 wt%. The morphology and bulk and surface properties of these nanocomposites have been studied in our previous papers [22, 23], using XDR, SEM, TEM, FTIR, contact angle measurements, etc. The main characteristics are briefly summarized here for to show their interdependence, which explains the effect of nanoparticle content on thermal behavior.

A previous paper [19] analyzed the existing interactions between the hydroxylic oxygen of two polymers and ammonium ions from the silicate galleries, in composites containing Nanocor I28 [19]. The interaction forces, on the one hand, and the mechanical shear active during processing, on the other, interpose the polymer with the silicate and enlarge the silicate galleries. The hydrophilic character of the matrix assures a good miscibility with montmorillonites and an easy intercalation. The diffraction peaks are shifted toward small angles, the resulted materials behave as intercalated nanocomposites. Intercalation increased basal spacing from 9.76 to 10.53 nm for nanocomposites containing Nanocor I28 and from 5.36 to 8.62 for nanocomposites containing Peruvian clay. The nanoparticles are uniformly distributed in both phases of the blend at all contents of montmorillonites [23].

Investigation methods

Thermal degradation was followed by simultaneous TG/DSC-FTIR-MS thermal analyses. The thermal study was performed on a STA 449 F1 Jupiter apparatus (Netzsch, Germany). The heating program started from 30 °C up to 600 °C at a 10 °C min^{-1} heating rate, under nitrogen as a purge and protective gas for a flow rate of 70 mL min^{-1}. The temperature reproducibility of TGA was ±2 °C, and the non-volatile fraction was ±3 %. The thermobalance was coupled with a Vertex 70 IR spectrophotometer and an Aëolos QMS 403C mass spectrometer (Netzsch, Germany) for in situ recording of the spectral characteristics of the degradation gaseous products. For each recording, 7–8 mg of sample was placed in Al_2O_3 crucible. Temperature calibration was done with standard indium, zinc, tin, bismuth, and aluminum of 99.99 % purity. Volatile degradation products in a temperature controlled environment were directly transferred both to an electron impact ion source of a mass spectrometer QMS 403C Aëolos (Netzsch) type and to an infrared (FTIR) spectrometer, via a heated capillary tube and analyzed by in situ vapor phase FTIR. Transfer of the degradation gaseous products was realized through two isothermal lines.

Kinetic analysis considered that the solid samples were decomposed in solid residue and gas products. The overall kinetic parameters: pre-exponential factor (A), activation energy (E_a), and reaction order (n) were evaluated by integral methods using the "Versatile" commercial program that calculates the overall kinetic parameters by various methods. The kinetic parameters of the thermal decomposition that involves overlapped processes (decomposition, cross-linking between the carbohydrate polymer chains and between PVA and the carbohydrate polymer, or some of the thermal degradation products recombined during heating) were evaluated by Flynn and Wall method, which is considered the most suitable [24, 25].

Results and discussion

TG results

The thermograms are presented in Fig. 1 and the thermogravimetric data are summarized in Table 1. At least five thermogravimetric steps are found in the DTG curves of nanocomposites over the 30–600 °C temperature range.

The first mass loss step recorded on the TG curve is attributed to the evaporation/dehydration of the water adsorbed from nanocomposites, and its thermogravimetric characteristics are not listed in Table 1. The thermal stability of nanocomposites was appreciated by the temperature variation of 5 wt% ($T_{5\ \%}$) and 50 wt% ($T_{50\ \%}$) mass loss.

For instance, the temperatures at both 5 and 50 wt% mass losses of 2–4 wt% clay nanocomposites are higher than that of the PVA/starch blend and the carbonaceous residue is higher. Apparently, the thermal stability of nanocomposites is increased because of the presence of well-dispersed clay in the blend matrix at these Nanocor I28 contents. In the case of nanocomposites containing Peruvian clay, the situation is different, as it appears that only for a content of 3–4 wt% clay thermal stability slightly increases as $T_{5\ \%}$ and $T_{50\ \%}$ are higher, and also that the residue mass is higher than those found for nanocomposites with a different montmorillonite content. Above this Peruvian clay content, thermal stability decreases.

The results agree with those found by other authors [7, 26] for nanocomposites based on plasticized poly(*L*-lactide) [26], polyethylene [27], polypropylene [28, 29], and elastomeric polyurethanes [30]. According to the experimental results, at a higher Na^+-montmorillonite content, chain cleavage by the ester hydrolysis reaction was more pronounced, leading to the formation of much shorter PLA

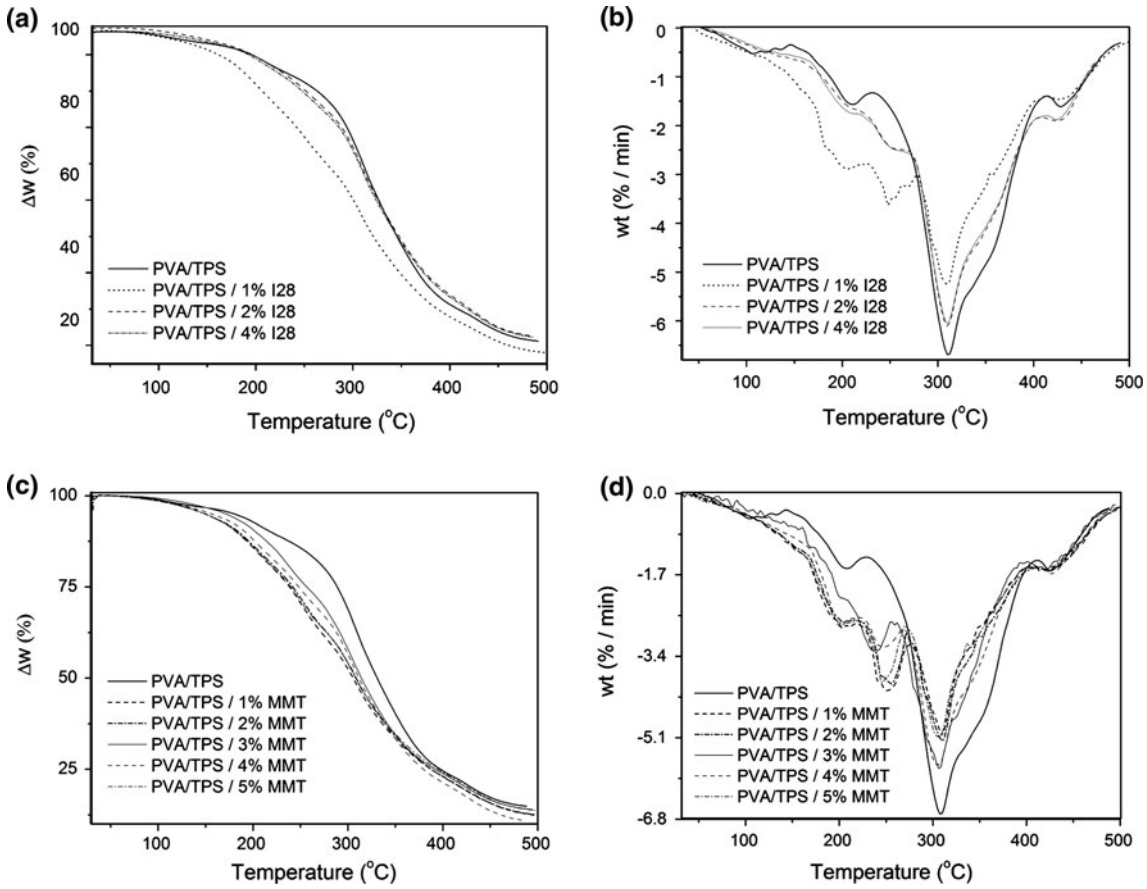

Fig. 1 Thermograms (TG) and derivative curves (DTG) of nanocomposites

Table 1 The thermogravimetric data for PVA/starch blend and nanocomposites

Nanoclay (wt%)	$T_{5\ \%}$ (°C)	$T_{50\ \%}$ (°C)	$\Delta W_{,\ 40 \div 550\ °C}$ (wt%)	Residue (wt%)	DTG peak temperature (°C)			
					Step 1	Step 2	Step 3	Step 4
PVA/TPS								
0	181.7	333.5	86.6	13.43	104; 204	–	311; 354[a]	428.3
PVA/TPS/I28								
1	161	308	89.6	10.40	205.3	247.8	310.3	425.8
2	184.3	333.9	85.8	14.19	208[a]; 218	251[a]; 260	312.5; 347	426.5
4	184	335.6	85.2	14.77	218	260	312.4	426.8
PVA/TPS/MMT								
1	152	308	88.7	11.28	203.8	252.5	312.7	416.6
2	152.9	311	88.8	11.62	206.9	257.5	312.5	426.1
3	175	317	86.8	13.18	–	244.7	309.6	422.3
4	160	314	86.2	13.83	203.4	251.9	308	429.3
5	153	311	87.2	12.78	206.5	248.3	309	425.6

[a] sh-shoulder on derivative thermogravimetric curve

$T_{5\ \%}$, $T_{50\ \%}$: the temperature corresponding to 5 and 50 wt% mass losses

chains [26] known to degrade at lower temperatures which could be true in our systems as well. Only a certain content of nanoclay assures enhanced properties.

The overall kinetic parameters of the main decomposition steps were evaluated for the second step, occurring in 130–235 °C range and for the third one, which occurs in

the 235–410 °C range, respectively. In the second process, a change in the reaction order occurs which decreases in the case of nanocomposites decomposition, probably because of the influence of diffusion. The activation energy takes a higher value than that corresponding to the blend only for nanocomposites containing 2–4 wt% Nanocor I28, while Peruvian clay (untreated montmorillonite) seems to have a catalytic effect on thermal decomposition, because the activation energies of decomposition of these nanocomposites have lower values than that of the PVA/starch blend. The changes in thermal properties observed in a nitrogen atmosphere are smaller than those obtained in air, previously presented [31].

In the third step of mass loss, the reaction order is 1.9–2.0 for nanocomposites' decomposition, which is higher than that found for the PVA/starch blend of 1.5–1.7.

The overall activation energy and the corresponding pre-exponential factor took higher values for all nanocomposites with respect to the blend values. It can be assumed that the other reactions are overlapped on those of components' decomposition.

Analysis of the evolved gas products

FTIR results

The evolved volatile compounds are characterized using in situ vapor phase FTIR as a function of the mass loss/degradation temperature for each nanocomposite sample. Figure 2 shows the vapor phase 3D FTIR spectra of PVA/starch blend and nanocomposites with different contents of nanoparticles. The 3D FTIR spectra presented in Fig. 2 show that volatile compounds emission during degradation of the PVA/starch blend appears as a complex process developed over a wide temperature range, while for nanocomposites decomposition, volatile compounds' evolution occurs in distinct steps.

Some differences in the peak positions and in relative intensities appear, as well as new bands, implying that the thermally-degraded compounds are qualitatively and quantitatively specific to each clay content and each decomposition step. An important amount of decomposition products was evolved after 23 min ($T = 186$ °C) of heating, and the compounds containing functionalities appearing at around 1,720–1,768 cm^{-1} slowed down, while the compounds with OH, C–O, and CH_3 functionalities evidenced by bands at 1,120–967 cm^{-1} increased (Fig. 2a). For a content of 1–2 wt% Nanocor I28, nanocomposites show mainly the same characteristics as the blend with some small additional bands (Fig. 2b); while, at a higher Nanocor I28 content, this delays a little decomposition ($\sim$26 min) ($T = 211$ °C). Generally, the 3D FTIR spectrum preserved the main bands found for the decomposition products of the blend, but at different intensities (Fig. 2c).

In the case of nanocomposites containing Peruvian clay, the 3D FTIR spectra show important differences (Fig. 2d, f) in the bands in the 2,250–2,357 cm^{-1} region corresponding to the P and R branch of CO_2, increasing during decomposition. FTIR bands appear even at the beginning of the process, with the exception of nanocomposites containing 3 wt% Peruvian clay where the start seems to occur after 20–21 min, while for a content of 5 wt% Peruvian clay, the volatile compounds appear after 11 min (Fig. 2f) ($T = 89$ °C).

The bi-dimensional spectra presented in Fig. 3 and the assignment of significant bands summarized in Tables 2 and 3, lead to the following observations. Bands assignment was done according to literature data and to the mechanism of PVA and starch decomposition [32, 33]. Gilman et al. [32] showed that degradation of the PVA samples starts at onset decomposition temperature around 204–218 °C with hydroxyl groups elimination due to the dehydration, followed by polyene formation around 300 °C as well as formation of aldehydes/ketones and benzene derivatives. The chemical reactions of thermal decomposition of starch, initiated around 300 °C, generated ether and ethylene segments via thermal condensation and dehydration mechanisms [34]. Heating to higher temperatures generates substituted phenol/benzene and furan structures with methylene and other linkages between these aromatic rings [35]. Above 400 °C, the starch structure was destroyed and the products appeared structurally similar to thermal cross-linked/decomposed phenol/furfural alcohol resins [36]. The main volatile products were polar oxygenated and carbon dioxide and water. The following decomposition products have been identified: formaldehyde, formic acid, acetic acid, propionic acid, CO_2, methane, traces of methanol, CO, CH_4, furan, acetone, 2-methylfuran, 2-furaldehyde, 2,5-dimethylfuran, 2-propanone, and butyraldehyde.

To follow the progress of degradation, the in situ vapor phase FTIR spectra for the evolved products, at 5, 20, and 50 wt% mass loss of the PVA/starch blend (Fig. 3a) and of nanocomposites (Fig. 3b–f) are plotted in Fig. 3, which depicts the changes induced in the composition of the products during decomposition. In all cases, the composition of the volatile products was changed according to the extent of degradation and the FTIR spectra being specific to each step and each studied system. At high clay content and prolonged degradation, the composition of the volatile products became much more complex.

The antisymmetric stretch of the CH_2 groups at 2,910 cm^{-1}, absorption of ester groups at 1,736 cm^{-1}, and stretching vibrations at 1,508 cm^{-1} characteristic to aromatic C=C bonds present significant increase in intensities

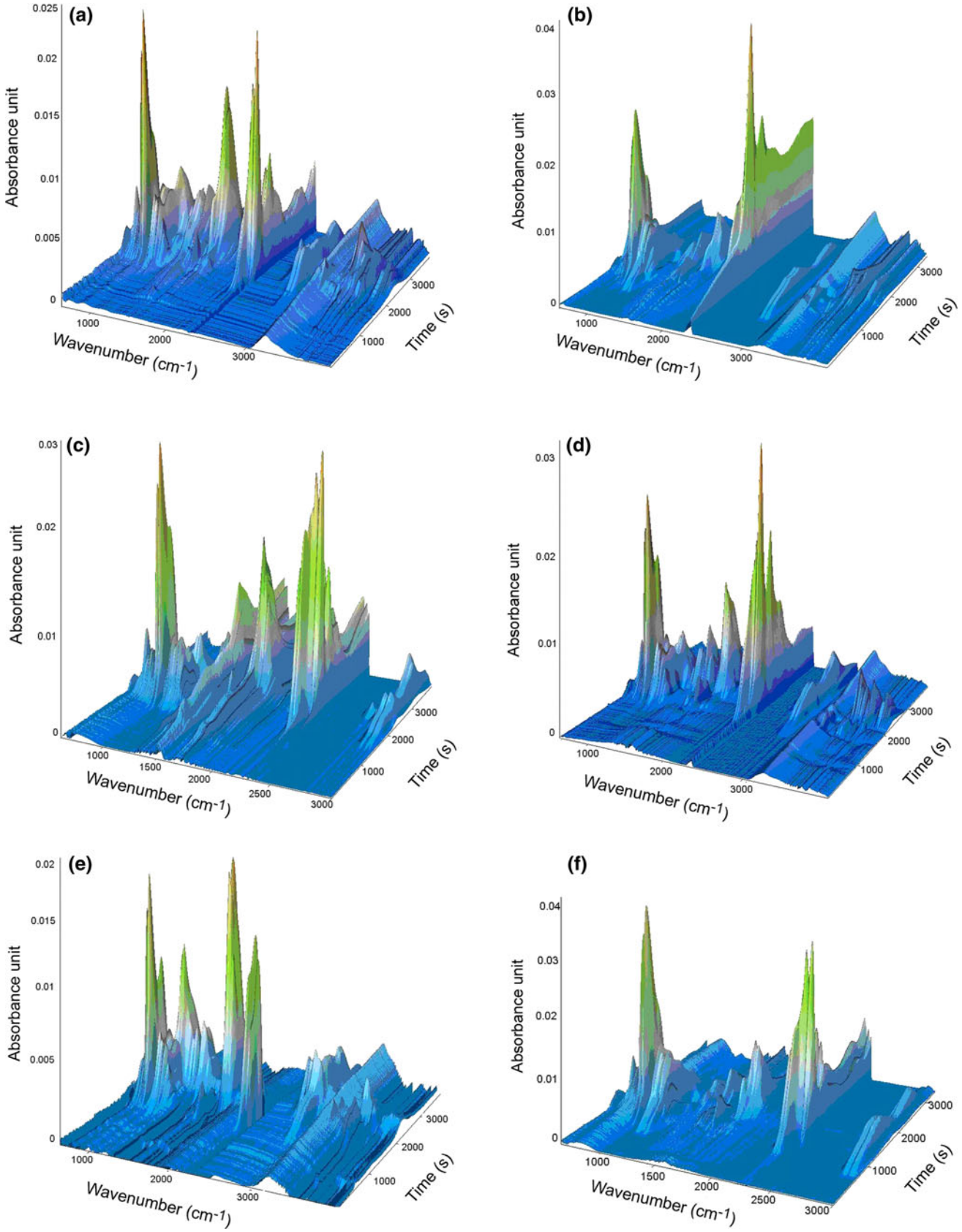

Fig. 2 3D FTIR spectra of the thermal decomposition of 50 % APV/50 % starch blend and of nanocomposites with different nanoclays content: **a** PVA/TPS, **b** PVA/TPS/2 wt% I28, **c** PVA/TPS/4 wt% I28, **d** PVA/TPS/1 wt% MMT, **e** PVA/TPS/3 wt% MMT, and **f** PVA/TPS/5 wt% MMT

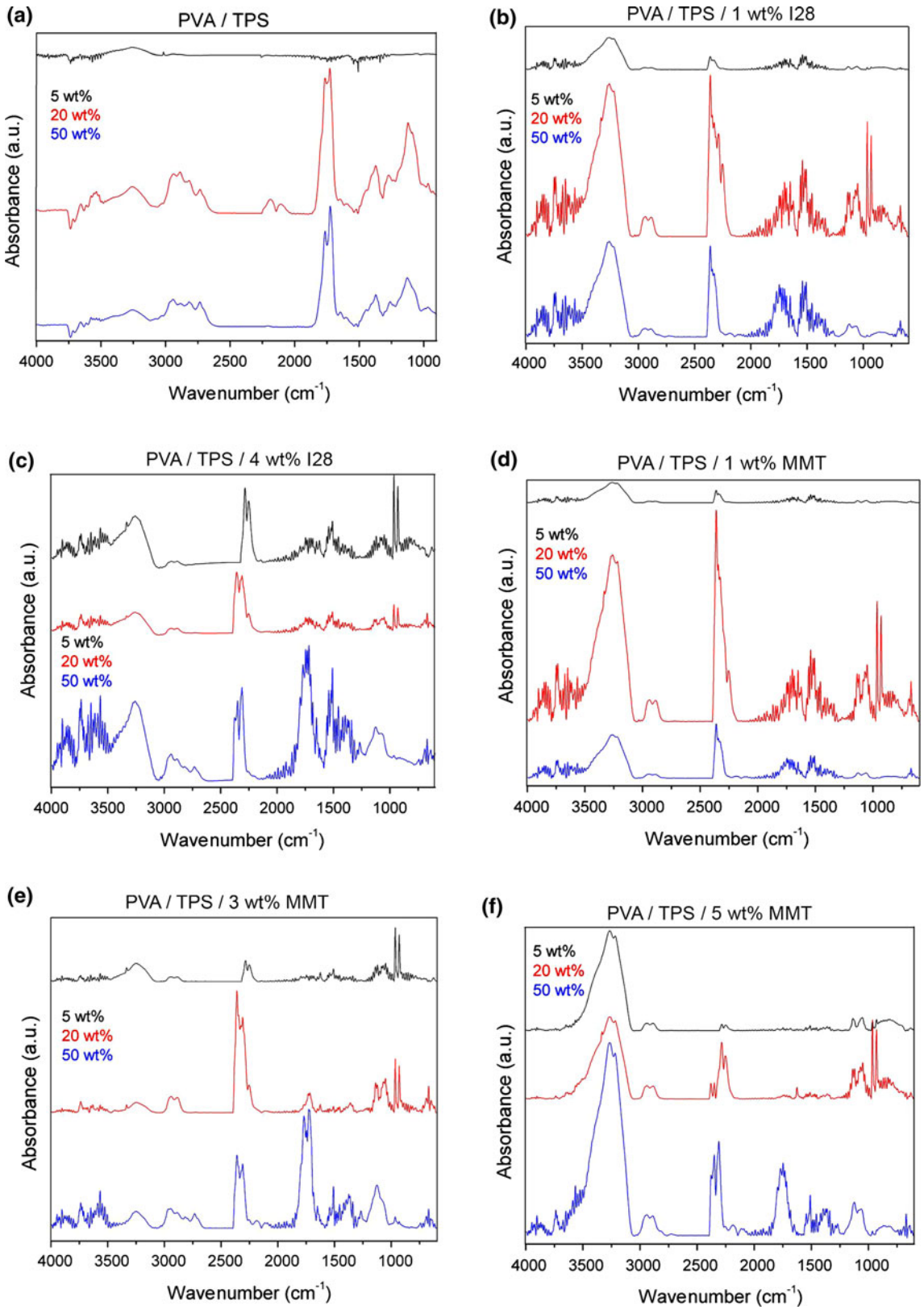

Fig. 3 In situ vapor phase FTIR spectra at 5, 20, and 50 wt% mass loss for PVA/starch blend and nanocomposites containing various amounts of Nanocor I28 (**a–c**) or Peruvian clay (**d–f**)

Table 2 The FTIR absorptions bands of in situ vapor phase for the poly(vinyl alcohol)/starch blend and nanocomposites containing Nanocor I28

5 wt% PVA/TPS	20 wt%	50 wt%	5 wt% PVA/TPS/1 wt% I 28	20 wt%	50 wt%	5 wt% PVA/TPS/4 wt% I 28	20 wt%	50 wt%	Assignment
3,770–3,669 vw	3,654–3,541 w	3,666–3,576 vw		3,737 m	3,737 m	3,737 w	3,737 w	3,732 m	–OH; C–H from acetic acid
						3,565 vw	3,565 vw	3,565 w	–OH from carboxylic acid, methanol, propanol
						3,336 w	3,332 w		–OH from 2-propanone and carboxylic acids or methanol, –C–H from alkynes
	3,262 w	3,260 vw	3,264 m	3,253 s	3,253 s	3,253 m	3,264 w	3,258 m	–OH, hydrogen bonded
	3,080–2,589 m	2,943–2,729 w		2,936; 2,884 m split	2,946; 2,884 w split	2,934; 2,887 vw	2,934; 2,879 vw	2,938; 2,887 w	C–H deformation sym; C–H (formaldehyde, butyraldehyde, acetone, formic acid, acetic acid, alkynes, methane, furan), antisymmetric stretch of CH_2 groups in aldehydes,=C–H
	2,935–2,792 m							2,730 w	C–H deformation; asym. (butyraldehyde, methanol); –C–H (formaldehyde, acetone)
			2,362 w	2,358 s	2,358 s				CO_2
				2,286 s		2,281 s	2,357 s	2,375 m	CO_2
2,221 vw	2,185 vw			2,249 m		2,252 s	2,310 s	2,351 s	P and R branch CO_2
								2,310 s	C≡C medial alkyne
	2,098 vw			2,111 w	2,099 w				CO; vC≡C alkyne
	1,768 s	1,764 s			1,749 m				C=O anhydride or acid (formaldehyde and acetic acid, acetone skeletal vibration)
	1,722 s	1,722 s				1,710 w	1,715 vw	1,793–1,683 m; 1,715 s	C=O (anhydride, acetic acid, carboxylic acid, acetone 2-propanone), one or more esters
	1,645 vw	1,643 vw		1,646 w				1,650	C=C stretch; The carbon–carbon double bond stretching at 1,630 cm^{-1} and the C–H out-of-plane deformations
1,598 vw	1,593 vw	1,593 vw							C–C skeletal vibrations of the ring from starch
	1,525 vw		1,541 vw	1,541 m	1,541 m	1,508 w	1,508 vw	1,508 m	Aromatic stretching of benzene ring; phenolic C–O band. CH_2 (formaldehyde) C–H def. methane, aromatic C=C bonds
1,479 vw									CH_2, scissoring (formaldehyde); C–H (alkyne) CH_3 def. acetic acid; –OH asym. (methanol)
	1,374 m	1,370 m							C–H bending or wagging, CH_3; –OH (methanol; C–H methyl alkynes, formic acid, acetic acid)
	1,273 m	1,260 w							CH_2 rock. (formaldehyde); –OH bend acetic acid
	1,120 s	1,131 m	1,136 vw	1,136 m	1,125 w	1,136 w		1,121 w	C–O stretching (alcohol, 2-propanone); CH_3 methanol
				1,047 m	1,063 w				C–O–H stretching; C–O methanol, C–H bend, rock (formic acid, acetone, furan)
967 vw	967 w	959 vw		964 s		964 s	964 w		C–O–C
928 vw				927 s		929 s	929 w		C–O–C skeletal mode vibrations of α-1,4 glycosidic linkage from starch
				667 w	667 w		670 w	667 w	C–C skeletal mode vibrations

Table 3 The FTIR absorptions bands of in situ vapor phase for the nanocomposites containing Peruvian clay

5 wt% PVA/TPS/1 wt% MMT	20 wt%	50 wt%	5 wt% PVA/TPS/3 wt% MMT	20 wt%	50 wt%	5 wt% PVA/TPS/4 wt% MMT	20 wt%	50 wt%	5 wt% PVA/TPS/5 wt% MMT	20 wt%	50 wt%
	3,737 m	3,737 w		3,737 w	3737 w	3,737 w	3,737 w	3,732 m			3,737 w
			3,332 w	3,332 w	3565 m				3,258 s	3,264 s	3,264 vs
3,264 m	3,253 s	3,264 m	3,248 m	3,253 w	3248 w	3,248 vw	3,243 vw	3,248 w	3,212 s	3,212 s	3,217 vs
	2,936; 2,884 m split	2,946; 2,889 vw split	2,941; 2,884 vw split	2,936; 2,884 w split	2,957; 2,884 w split		2,941; 2,889 w split	2,936; 2,889 m split	2,936; 2,884 w split	2,941; 2,879 w split	2,941; 2,889 m split
					2,733						
2,358 w	2,358 w	2,358 w		2,358 vs	2,358 s	2,358 m	2,358 s	2,358 vs		2,379; 2,348 w split	2,379; 2,348 m split
2,338 w			2,886 m	2,307 s	2,307 s	2,338 w		2,338 vs			2,307 s
	2,255 m		2,249 w	2,255 m			2,286 m		2,286; 2,244 w split	2,286; 2,249 m split	
					2,176 vw			2,176 w			2,181 w
		1,749 w		1,718 w	1,770 vs			1,746 m			1,749 m
	1,698 m				1,724 vs	1,708 vw	1,698 vw				
										1,625 vw	
1,520 vw	1,541 m	1,541 w	1,505 vw		1,510 m	1,541 vw	1,536 vw	1,541 m			1,510 m
					1,370 m						1,370 w
	1,141 m	1,131 vw		1,136 m	1,125 m			1,125 m	1,136 w	1,136 w	1,120 m
	1,047 m	1,057 vw	1,047 vw	1,042 m			1,052 w	1,063 m	1,057 w	1,047 w	1,063 w
	964 s		964 w	964 vw	964 vw	964 m	964 m		964 vw	964 s	
	927 m		927 w				927 m		828 vw	927 s	870 vw
	667 w	667 vw		667 vw	667 vw	667 vw	673 w	667 m			667 w

with increasing the Nanocor I28 content in nanocomposites' composition (Fig. 3b, c).

These bands correspond to C–H symmetric deformation, C–H vibration (formaldehyde, butyraldehyde, acetone, formic acid, acetic acid, alkynes, methane, and furan) and aromatic stretching of benzene ring, phenolic C–O band, CH_2 (formaldehyde), and C–H deformation in methane, respectively, even if some of them are overlapped. In the case of PVA/starch blend, the vapor phase FTIR spectra at 5 wt% mass loss show two bands at 1,598 cm^{-1} assigned to C=O, asymmetrical C=C and at 1,472 cm^{-1} for C–H wagging vibrations from the PVA component of the blend which do not appear any more, during prolonged thermal decomposition. Only for an extent of 20 wt% decomposition, new bands are presented in FTIR spectrum at 2,185 and 2,098 cm^{-1} assigned to alkyne bonds, but these bands disappear at high extent of decomposition. The characteristic bands for both 20 and 50 wt% decomposition appear at 1,366, 1,279, and 1,116 cm^{-1}, corresponding to CH_3 symmetric deformation, to C–O in alcohol groups, CH_2 in formaldehyde, and C–H alkyne; the splitted band at 1,770 and 1,722 cm^{-1} is very strong being assigned to C=O bonds in anhydride, carboxylic acids, butyraldehyde, and 2-propanone; while the broad bands at 3,080–2,589 cm^{-1} and 3,253–3,262 cm^{-1} can be assigned to carboxylic acid and water, respectively.

Hydroxyl stretching also shows two regions of bands at 3,534–3,566 cm^{-1} and 3,400–2,400 cm^{-1} (very broad, with maxima at 3,257 cm^{-1}), while secondary and primary OH in-plane bending and O–H groups appear at 1,271 cm^{-1}.

The spectra plotted in Fig. 3 show a broad band centered near 3,250 cm^{-1}, which is due to the hydrogen bonded O–H groups. It seems that some condensed phase material is deposited on the windows of their flow cell. These bands are more intense at a mass loss of 20 and 50 wt% in spectra of volatile phase evolved from the nanocomposites containing 2–4 wt% Nanocor I28. The 1,271 cm^{-1} absorption band is also attributed to the aromatics, ethers which appear at high temperature. Hydroxyl stretching shows enhanced intensity in the early decomposition stages, as a consequence of degradation of the poly(vinyl alcohol) chain, accompanied by hydroxyl compounds release and formation of polyene. Also, the absorption bands at 2,815 and 2,733 cm^{-1} are attributed to the C–H stretching mode of aldehydes. The carbonyl stretching region of the IR spectra presents two absorption bands at 1,730 cm^{-1} and, respectively, at 1,124 cm^{-1}, for the ether group. The anhydride –C=O group formed at high temperature is present at 1,760 cm^{-1}, and it is shifted at 1,766 cm^{-1} at 50 % mass loss. The 1,768 and 1,722 cm^{-1} and also 1,643–1,647 cm^{-1} bands assigned to the C=O of the ester, anhydride, or acid, present only at high mass loss, are shifted to lower wavenumbers in the spectra of the products resulted from nanocomposites with 3–4 wt% Nanocor I28.

When temperature increases up to 300 °C, starch suffers a thermal condensation between the hydroxyl units of chains, forming ether and ethylene segments and eliminating water and the small molecular species. Dehydration of the neighboring hydroxyl groups in the glucose ring of starch leads to the formation of C=C bonds or breakdown of the glucose ring [33]. If the glucose ring is broken down, then aldehyde groups may be formed. Skeletal C–C vibration of the starch ring at 1,593 cm^{-1} appears only in volatile decomposition products from the blend, and it is not evident in the FTIR spectra of the products resulting from nanocomposites. This should mean that nanoparticles act mainly on starch decomposition.

The noise-like bands at 1,400–1,900 and 3,500–3,900 cm^{-1} are due to H_2O evolution, and the shoulder-like band around 1,620 cm^{-1} corresponds to the carbon–carbon double bond stretching. Carbon dioxide presence in volatile products evidenced by the bands at 2,360–2,320 and 670 cm^{-1} is observed mainly in products resulted from nanocomposites at longer decomposition periods. In the case of products from nanocomposites, the band attributed to carbon dioxide is split and it presents many shoulders.

Heating at increased temperature generates aromatic rings, such as benzene or furan structures linkages (either $–CH_2–$ or $–CH_2–O–CH_2–$) between the aromatics groups. The C–H stretching of the $–CH_2–O–$ group is also responsible for band absorption at 2,815 cm^{-1}. Methyl C–H bending at 1,371 cm^{-1} is not found any more in products from nanocomposites, while the C–C skeleton vibration at 1,048–1,063 cm^{-1} is found only in nanocomposites with low content of Nanocor I28 clay. The additional IR absorption bands for nanocomposites are due to the influence of nanoparticles on poly(vinyl alcohol)/starch decomposition and to the interactions created between the compounds during thermal degradation. The 667 cm^{-1} band appears only in spectra of the nanocomposites decomposition products, at high mass losses.

In the case of nanocomposites containing Peruvian clay, important differences in the FTIR spectra of the volatile decomposition products with respect to the PVA/starch blend depending on the content of incorporated nanoclay are evident. The main bands of the spectra of nanocomposites with 1 wt% Peruvian clay are: 3,250 cm^{-1} (O–H groups, bonded hydrogen), 2,371 cm^{-1} (CO), 1,659 cm^{-1} (C=C), and 1,486 cm^{-1} (aromatic stretching) which show the highest intensities at 20 wt% mass loss. The band at 927 cm^{-1} disappears in the spectra corresponding to a mass loss of 50 wt% from the nanocomposite. The spectra of the nanocomposite with 3 wt% Peruvian clay show only a weak band at 3,526 cm^{-1} (50 wt% mass loss); new

bands are present at 3,256, 2,946, and 2,929 cm^{-1}. The band at 2,236 cm^{-1} is shifted to 2,352 cm^{-1} and a strong band appears at 1,755 cm^{-1} and at a high mass loss of 50 wt%. The bands at 1,082 and 908 cm^{-1} at 5 and 20 wt% mass losses are not present, any more, in the spectrum at 50 wt% mass loss, but a new band appears in this case at 1,120 cm^{-1}, which should mean that MMT nanoclay promotes formation of carbonyl, carboxyl, and unsaturated structures. The products resulted from nanocomposites containing 5 wt% Peruvian clay become more complex at longer decomposition, by formation of new functionalities with characteristic bands at 1,736, 1,486, and 1,351 cm^{-1}. The wide band at 3,237 cm^{-1} is present in all three spectra.

The TG/FTIR study on nanocomposites degradation revealed some changes, caused by the influence of the nature and content of nanoclay. The intensity of the sp^3 carbon–hydrogen stretching vibration increases as the clay content increases, especially for the band at 2,970 cm^{-1} which is assigned to the sp^3 carbon–hydrogen (methyl) stretching for both kinds of nanoclays used, while the bands at 990 and 910 cm^{-1} increase with the Nanocor I28 content and decrease with the Peruvian clay content. As the clay content increases, the number of peaks increases and therefore, many additional structures may be counted. Similar observations about the changes observed in the composition of the volatile decomposition products caused by the nature and content of clay of nanocomposites have been mentioned by other authors for different synthetic nanocomposites [37].

MS results

Based on the literature data and on the decomposition mechanism of PVA [32, 38] and starch [36, 39, 40], the following possible decomposition products have been identified in FTIR and MS spectra (Table 4). FTIR spectra absorption bands and mass spectroscopy results assignments were performed according to the NIST spectra database and other databases [41, 42].

Table 4 shows the m/z ratios of the possible ionic fragments resulted from the thermal decomposition of PVA/starch blend and nanocomposites and their assignments [41, 42].

The Peruvian clay nanoparticles induce changes in the thermal degradation of the nanocomposites, as evidenced by the new ionized fragments at 93 and 96. The m/z ratios correspond to the aromatic ether [43]. The ion masses related to the hexanal from starch have a signal at $m/z = 83$ [44]. The evolution, during heating or with temperature, of some of the most representative ionized fragments of various possible gaseous decomposition compounds is plotted in Figs. 4 and 5.

Table 4 The m/z ratios of the possible ionic fragments formed from thermal decomposition of PVA/starch blend and nanocomposites and their assignments [41, 42]

Assigned compound	The m/z of the possible ionic fragments formed from different compounds (in order of decreasing intensity)
Formaldehyde	29, 30, 28, 15, 12, 13, 14
Formic acid	29, 46, 45, 29, 17, 43
Acetic acid	43, 45, 60, 15, 29, 42
Methanol	31, 32, 29, 15, 30
Acetone	43, 58, 15, 42, 14
CO_2	44, 28, 16, 12, 45
H_2O	18, 17, 16
Ethylene	28, 27, 26, 25, 14
Propionic acid	74, 45, 28, 29, 27, 57
Methane	16, 15, 14, 13, 12
Furan	68, 39, 38, 40, 29
2-Furaldehyde	96, 95, 39, 38, 29, 67
2.5-Dimethylfuran	96, 95, 81, 43, 53
Butyraldehyde	44, 43, 72, 29, 27
Benzene	73, 72, 46, 51, 63
Alkyne fragments	51, 52, 53, 54
CH_3CO^+ (benzaldehyde)	77, 105, 106, 51, 43
Polyene	56, 57
Methyl-terminated polyene, cis and trans	67, 69, 70
Hexanal	44, 56, 41, 29, 72, 82
Tropylium ion (from benzene alkyl substituents)	91, 120
Tropylium ions with alkyl substituents	105, 106
Aromatic ether	31, 51, 69, 93, 96

The $m/z = 15$ signal (Figs. 4a, 5a) can be attributed to numerous compounds, such as formaldehyde, formic acid, acetic acid, methane, methanol, or acetone; therefore, the variation during decomposition depends on nanoclay type and content. The mass spectra for the blend present only a peak at a maximum temperature of about 328 °C and the curve of the nanocomposites with Nanocor I28 shows two peaks centered at 247 and 318 °C, while the curves of the nanocomposites containing Peruvian clay indicate that the evolution of these compounds starts at about 60–80 °C and continues up to high temperatures of 400 °C. As to the influence of the nanoclay content, for Nanocor I28-containing nanocomposites, both the maximum temperature of evolution and the time to start release of these compounds increase with the Nanocor I28 content, while for nanocomposites containing Peruvian clay, both these values decrease with increasing the MMT content, with the exception of nanocomposite containing 3 wt% MMT, for

which the values are close to that of the blend or are slightly higher.

Variation of m/z = 16 (Figs. 4b, 5b) which could appear from methane, methanol, and CO_2, occurs as a complex curve with several maxima placed between 140 and 390 °C. These products are formed by PVA/starch blend and nanocomposites decomposition. The most complex one is the curve corresponding to the decomposition compounds of nanocomposites containing Peruvian clay. A similar variation is characteristic to formic acid formation of m/z = 17 signal (Fig. 4c) which has a maximum temperature at 310 °C from the decomposition of blend and nanocomposites with Nanocor I28, while the maximum is found at low temperature of 206–243 °C in

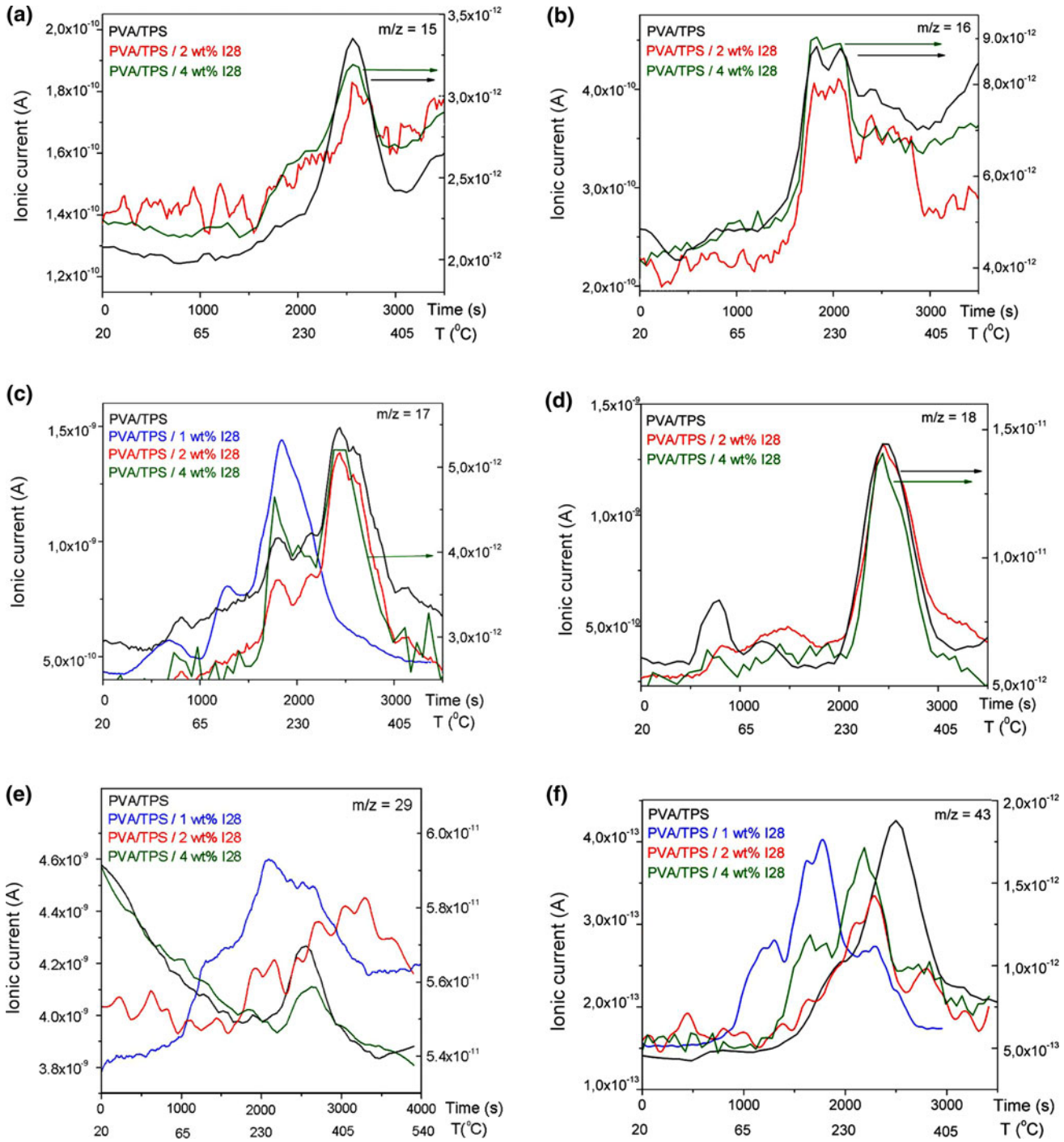

Fig. 4 Variation during decomposition of the relative intensity of the m/z signal corresponding to the most probable decomposition compounds identified in the MS spectra of PVA/starch blend and Nanocor I28 containing nanocomposites

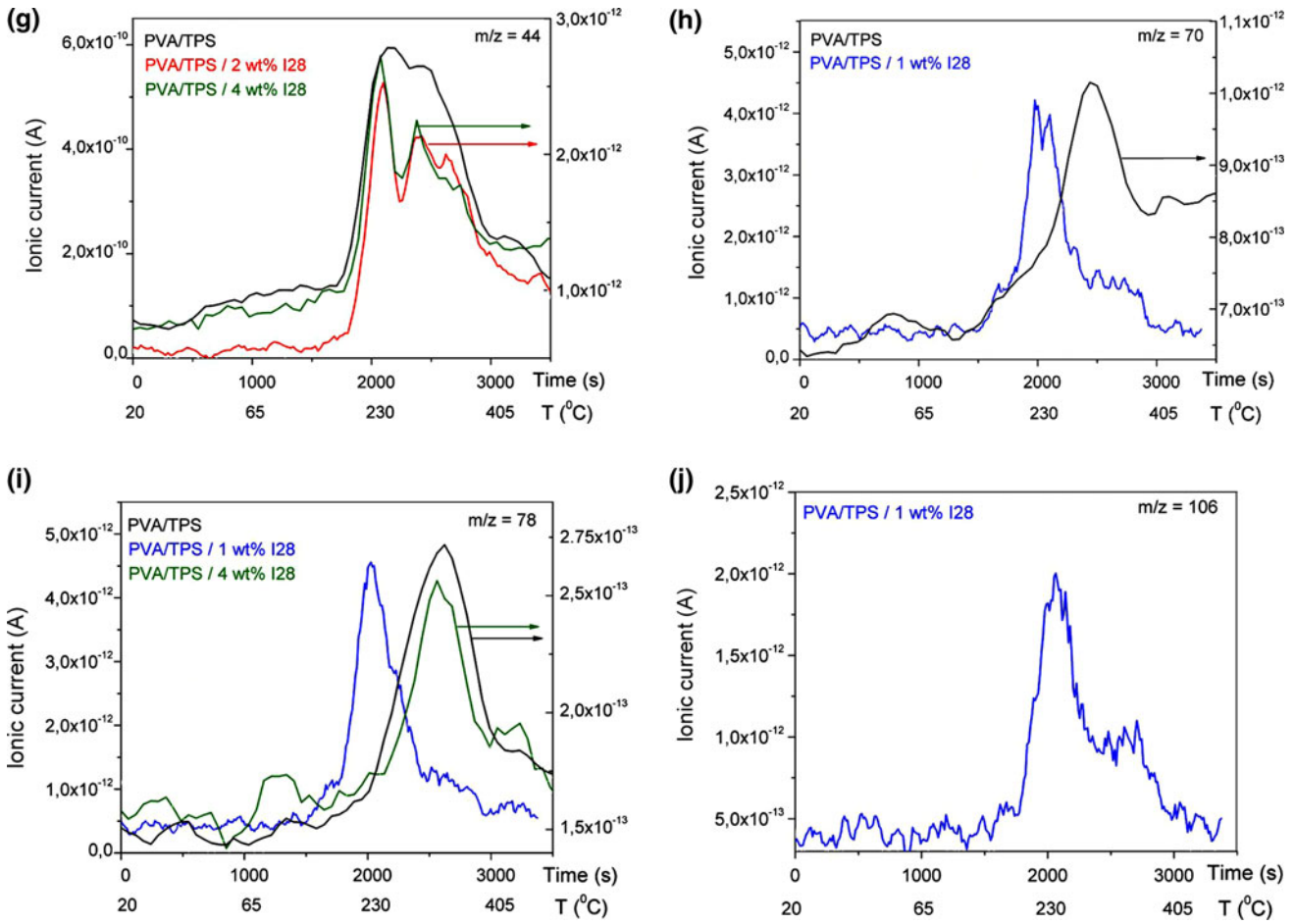

Fig. 4 continued

the cases of nanocomposites containing Peruvian clay. Variation with the nanoclay content is similar to that described for the m/z = 15 signal.

The curve of the m/z = 18 signal (Figs. 4d, 5c) assigned to water evolution starts at lower temperature, from the blend and composites containing Peruvian clay in low amounts. The maximum temperature of water release is 310 °C for the blend and nanocomposites containing Nanocor I28, and about 210 °C for the other nanocomposites. Peak height decreases with increasing the Nanocor I28 content, while the time for initiating the evolution increases and also does that of the nanocomposites with 3 wt% MMT. The m/z = 29 corresponds to formaldehyde elimination, and this is evolved faster from nanocomposites containing 1–2 wt% Nanocor I28 (Fig. 4e) at around 230–250 °C, followed by elimination at high temperatures of ~320 °C.

The formaldehyde, propionic acid, and methanol give fragments with m/z = 29 and 30 (Fig. 5d, e), evolved at temperatures of 90–150 °C from nanocomposites containing Peruvian clay, and at a temperature higher than 249 °C from the PVA/starch blend vary in low amounts from nanocomposites containing Nanocor I28. Acetone and acetic acid which correspond to a m/z = 43 (Fig. 5f) are formed and evolved in two stages, at maximum temperatures of 230 and 340 or 405 °C for the blend and nanocomposites containing Peruvian clay, while for nanocomposites containing Nanocor I28, the maximum temperature exceeds 300 °C and it is close to those of the second evolution stage of these compounds from the blend. This temperature remains constant for all Nanocor I28-containing nanocomposites, while the time for initiation of evolution increases. The compounds with characteristic m/z = 44 (Figs. 4g, 5g) mainly assigned to carbon dioxide, evolve in two or three steps, starting from temperatures of 155–200 °C for nanocomposites containing Peruvian clay and from 260 to 350 °C, respectively, for blend and nanocomposites containing Nanocor I28. The time of evolution initiation is longer for an increasing Nanocor I28 content and shorter for an increasing MMT content.

Polyene formation is an important step in the mechanism of PVA decomposition. Fragments with polyene structure are formed from blend and nanocomposites with Peruvian clay, but not from nanocomposites containing Nanocor I28 in a content higher a 1-wt% (Fig. 5h). Such compounds are

evidenced at m/z = 56, being assigned to –OH terminated polyene fragments and at m/z = 70 (Figs. 4h, 5i) being assigned to methyl-terminated polyene. The maximum evolution rate is recorded at 340–400 °C, over a large temperature interval of 150–200 °C. The maximum evolution rate temperature is placed at lower temperature for nanocomposites with respect to that of the blend, even at 200 or 250 °C for nanocomposites with Peruvian clay for m/z of 56 and 70 signals, respectively. The m/z = 78 corresponding to benzene varies according to a curve reaching

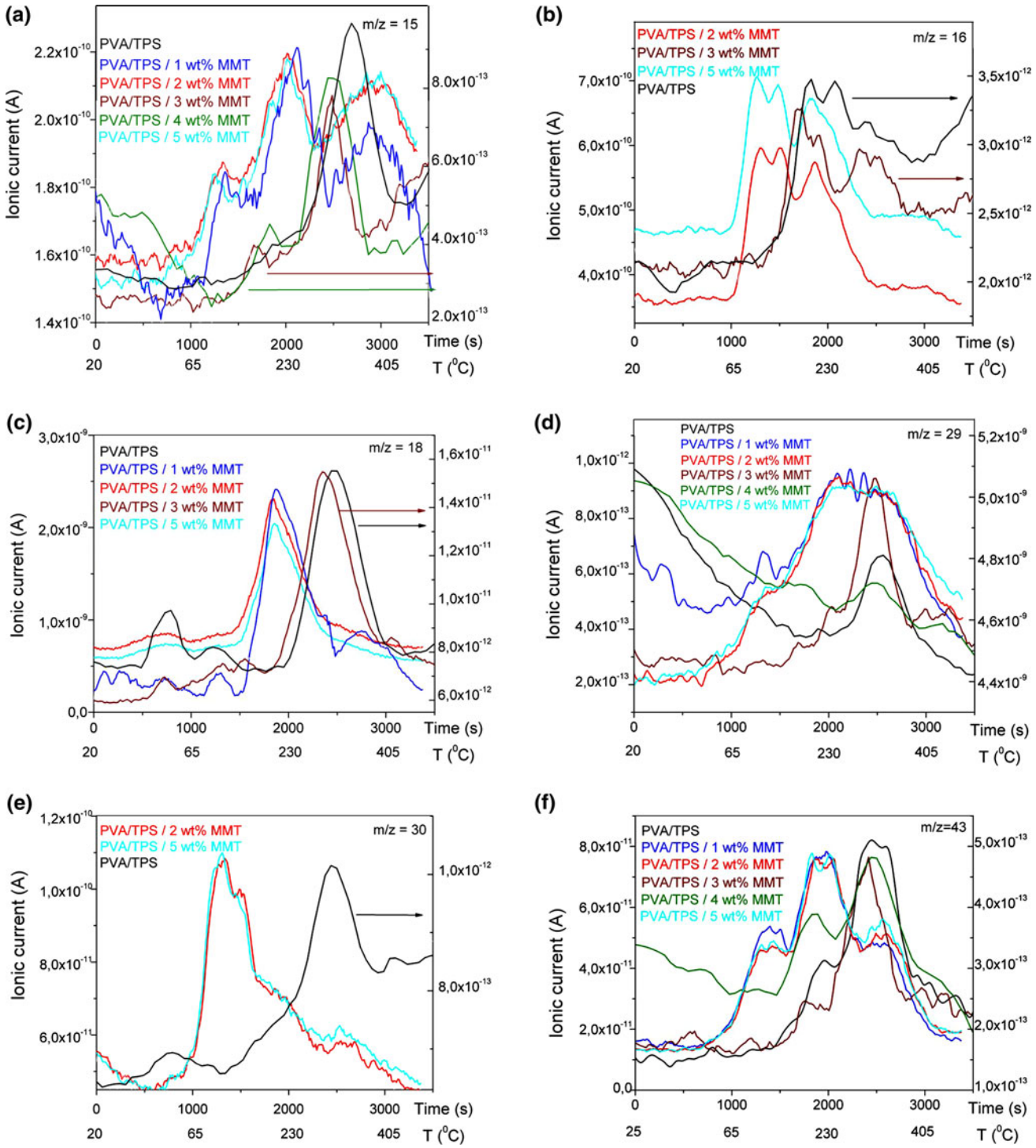

Fig. 5 Variation during decomposition of the relative intensity of the m/z ratio corresponding to the ionic fragments resulted from the most probable decomposition compounds identified in the MS spectra of PVA/starch blend and nanocomposites containing Peruvian clay

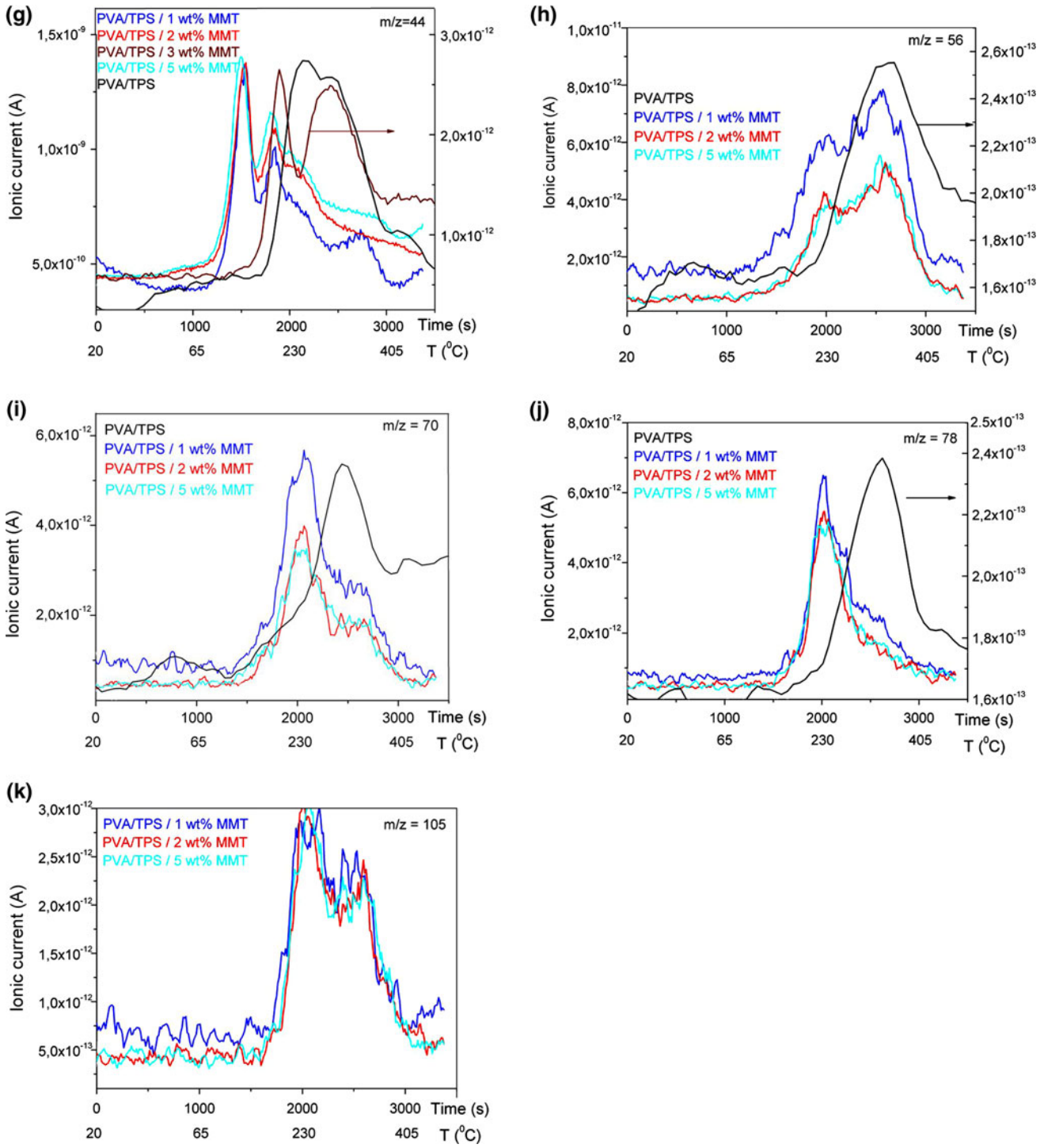

Fig. 5 continued

its maximum at a temperature of 200–230 and 340 °C for nanocomposites and PVA/starch blend, respectively (Figs. 4i, 5j). This compound is not present in decomposition compounds of nanocomposites with 2 wt% Nanocor I28. It appears at lower temperatures, increasing the Nanocor I28 content and at delayed starting evolution. The 2-methyl furan with main m/z = 83 starts to be released at low temperature from nanocomposites containing Peruvian clay, while it appears at temperature >400 °C from blend decomposition.

The compounds with m/z = 105 or 106 signals (Figs. 4j, 5k) are present only in decomposition compounds

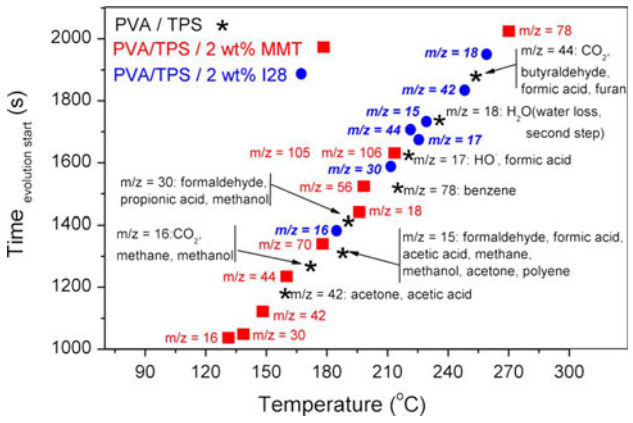

Fig. 6 Evolution of the gaseous phase for PVA/starch blend (PVA/TPS) and nanocomposites containing Nanocor (PVA/TPS/I28) and Peruvian clay (PVA/TPS/MMT)

of nanocomposites with Peruvian clay, when the maximum temperature of evolution is higher than 208 to 340 °C; while for other nanocomposites it is of 380 °C for the m/z = 106 signal. These signals can be assigned to substituted aromatics. Figure 6 presents the initiation time of various compounds' release in gaseous phase for PVA/starch blend and nanocomposites. The type of nanoclay influences the time of the start release of these compounds or the formation of other types of compounds (m/z of 83, 105 and 106), as a result of the secondary reactions of the degradation products at higher temperatures.

Jang et al. [45] established that, as the clay loading is increased, the evolved products formed through inter-chain reactions become significant. Due to the barrier effect of the clay layers, the radicals have greater chance to undergo radical transfer, producing tertiary radicals, and then radical recombination reactions, giving head–to–head structures; while hydrogen abstraction from the condensed phase also occurs. These reactions become significant at higher concentration of clay because the degrading polymer is retained by the clay layers, permitting further reactions. The radical recombination reactions induced by the presence of clay, cause retention of the degradation products for a longer period of time, thus spreading out the degradation in time and reducing the peak value. It is thought that inter-chain reactions become significant in the presence of clay because the degrading polymer chains are trapped in the gallery space of the clay during thermal degradation [46].

In accordance with the thermogravimetric results, Nanocor I28 incorporation leads to higher thermal stability and induces a delay in the release of the gaseous phase of decomposition; while MMT seems to promote decomposition mainly by easy release of the light compounds. The changes in decomposition compounds' composition could be due to the head-to-head structures, being possibly produced via radical recombination reactions, followed by extensive random chain scissions.

Conclusion

By in situ vapor phase FTIR and MS spectroscopic techniques, both the decomposition compounds of the constituent polymers and some new ones, depending on the nanoparticles content, are identified. The effect of the increase of the Nanocor I28 content consists mainly of longer evolution starting time of the volatile compounds, such as formic acid, water, formaldehyde, propionic acid, methanol, acetic acid carbon dioxide, benzene, etc. In the case of MMT-containing nanocomposites, variation of the time of the release (evolution) starting time is more complex. Most values remain below those corresponding to the blend.

A content of 2–4 wt% Nanocor I28 hinders the decomposition of PVA/starch blend, both characteristic temperatures of the main compounds evolution are increased by increasing the Nanocor I28 content and the starting time for their evolution is delayed; while in the case of nanocomposites containing MMT, this acts as a catalyst, decreasing the characteristic temperatures and evolution time with increasing the MMT content, with the exception of nanocomposites with 3 wt% MMT, for which the decrease is not so important.

The temperature dependence of the maximum evolution rate of various compounds on the nanoclay content is very complex as, in the case of nanocomposites, both primary and secondary reactions and also transport phenomena occur simultaneously. Generally, the thermal behavior of such polymeric nanocomposites containing montmorillonite is related to the organoclay content and to its dispersion in the matrix.

Acknowledgments Manuela-Tatiana Nistor thanks the financial support to Romanian National Authority for Scientific Research, CNCS–UEFISCDI, through PN-II-ID-PCE-2011-3-0187 project.

References

1. Suprakas SR, Masami O (2003) Polymer/layered silicate nanocomposites: a review from preparation to processing. Prog Polym Sci 28:1539–1641
2. Pielichowski K, Njuguna J (2005) Thermal degradation of polymeric materials. Smithers Rapra Publishing, Shawbury
3. Pielichowski J, Pielichowski K (1995) Application of thermal analysis for the investigation of polymer degradation processes. J Therm Anal 43:505–508
4. Ahmadi M, Moghbeli MR, Shokrieh MM (2012) Shrinkage and mechanical properties of unsaturated polyester reinforced with clay and core–shell rubber. Iran Polym J 21:855–868

5. Wu G, Yang F, Tan Z, Ge H, Zhang H (2012) Synthesis of montmorillonite-modified acrylic impact modifiers and toughening of poly(vinyl chloride). Iran Polym J 21:793–798
6. Leszczyńska A, Njuguna J, Pielichowski K, Banerjee JR (2007) Polymer/montmorillonite nanocomposites with improved thermal properties. Part I: factors influencing thermal stability and mechanisms of thermal stability improvement. Thermochim Acta 453:75–96
7. Guo B, Jia D, Cai C (2004) Effects of organo-montmorillonite dispersion on thermal stability of epoxy resin nanocomposites. Eur Polym J 40:1743–1748
8. Lim ST, Hyun YH, Choi HJ, John MS (2002) Synthetic biodegradable aliphatic polyester/montmorillonite nanocomposites. Chem Mater 14:1839–1844
9. Lim ST, Lee CH, Choi HJ, John MS (2003) Solid-like transition of melt-intercalated biodegradable polymer/clay nanocomposites. J Polym Sci Part B Polym Phys 41:2052–2061
10. Paul MA, Alexandre M, Degee P, Henrist C, Rulmont A, Dubois P (2003) New nanocomposite materials based on plasticized poly(*l*-lactide) and organo-modified montmorillonites: thermal and morphological study. Polymer 44:443–450
11. Hui-Wang C, Guan-Ben D (2008) Application of MMT in polyesters. Ind Mine Process 7:27–32
12. Hui-Wang C, Guan-Ben D (2009) Practice of PVAc type curing agent for UF resin in plywood production. Adhes in China 30:52–54
13. Patachia S (2003) Blends based on poly(vinyl alcohol) and the products based on this polymer, Chap. 8 in Handbook of polymer blends and composites, Vasile C, AK Kulshereshtha (Eds.). Rapra Technol 4A:285–365
14. Preechawong D, Peesan M, Rujiravanit R, Supaphol P (2004) Preparation and properties of starch/poly(vinyl alcohol) composite foams. Macromol Symp 216:217–227
15. Sreedhar B, Sairam M, Chattopadhhyay DK, Syamala RPA, Mohan Rao DV (2005) Thermal, mechanical, and surface characterization of starch/poly(vinyl alcohol) blends and borax-crosslinked films. J Appl Polym Sci 96:1313–1322
16. Follain N, Joly C, Dole P, Bliard C (2005) Properties of starch based blends. Part 2. Influence of poly vinyl alcohol addition and photocrosslinking on starch based materials mechanical properties. Carbohydr Polym 60:185–192
17. Cinelli P, Chellini E, Gordon SH, Imam SH (2003) Characteristics and degradation of hybrid composite films prepared from PVA, starch and lignocellulosics. Macromol Symp 197:143–156
18. Nistor M-T, Vasile C (2013) Influence of the nanoparticle type on the thermal decomposition of the green starch/poly(vinyl alcohol)/montmorillonite nanocomposites. J Therm Anal Calorim 111:1903–1919
19. Dimonie D, Constantin R, Vasilievici G, Popescu MC, Garea S (2008) The dependence of the XRD morphology of some bionanocomposites on the silicate treatment. J Nanomater, Article ID 538421
20. Dimonie D, Radovici C, Trandafir I, Pop SF, Dumitriu I, Fierascu R, Jecu L, Petrea C, Zaharia C, Coşerea R (2011) Some aspects concerning the silicate delamination for obtaining polymeric biohybrids based on starch. Rev Roum Chim 56:685–690
21. Dimonie D, Socoteanu R, Doncea S, Pop FS, Petre C, Dumitriu I, Fierascu R (2011) The miscibility estimation of some nanocomposites based on starch. e-Polymers 90
22. Dimonie D, Kelnar I, Socoteanu R, Darie RN, Pop FS, Zaharia C, Petrea C, Nemteanu M, Coserea RM (2010) The influence of miscibility and micro–structure on the surface defects of some starch bio–hybrides. Materiale Plastice 47:486–491
23. Pascu M-C, Popescu M-C, Vasile C (2008) Surface modifications of some nanocomposites containing starch. J Phys D: Appl Phys 41:175407
24. Flynn JH, Wall LA (1966) A quick, direct method for the determination of activation energy from thermogravimetric data. J Polym Sci Part B: Polym Lett 4:323–328
25. Vyazovkin S, Burnham AK, Criado JM, Pérez-Maqueda LA, Popescu C, Sbirrazzuoli N (2011) ICTAC Kinetics Committee recommendations for performing kinetic computations on thermal analysis data. Thermochim Acta 520:1–19
26. Paul MA, Alexandre M, Degee P, Henrist C, Rulmont A, Dubois P (2003) New nanocomposites materials based on plasticized poly(*L*-lactide) and organo-modified montmorillonites: thermal and morphological study. Polymer 44:443–450
27. Zhai H, Xu W, Guo H, Zhou Z, Shen S, Song Q (2004) Preparation and characterization of PE and PE-*g*-MAH/montmorillonite nanocomposites. Eur Polym J 40:2539–2545
28. Tang Y, Hu Y, Song L, Zong R, Gui Z, Chen Z, Fan W (2003) Preparation and thermal stability of polypropylene/montmorillonite nanocomposites. Polym Degrad Stabil 82:127–131
29. Qin H, Zhang S, Zhao C, Feng M, Yang M, Shu Z, Yang S (2004) Thermal stability and flammability of polypropylene/montmorillonite composites. Polym Degrad Stabil 85:807–813
30. Wang J, Chen Y, Wang J (2006) Preparation and properties of a novel elastomeric polyurethane/organic montmorillonite nanocomposite. J Appl Polym Sci 99:3578–3585
31. Vasile C, Stoleriu A, Popescu MC, Duncianu C, Kelnar I, Dimonie D (2008) Morphology and thermal properties of some green starch/poly(vinyl alcohol)/montmorillonite nanocomposites. Cell Chem Tech 42:549–568
32. Gilman JW, VanderHart DL, Kashiwagi T (1994) Thermal decomposition chemistry of poly(vinyl alcohol) char characterization and reactions with bismaleimides, Chapter 11 in Fire and Polymers. II: materials and test for hazard prevention. Am Chem Soc. ACS Symp Ser 599(11):161
33. Kizil R, Irudayaraj J, Seetharaman K (2002) Characterization of irradiated starches by using FT-Raman and FTIR spectroscopy. J Agric Food Chem 50:3912–3918
34. Zhang X, Golding J, Burger I (2002) Thermal decomposition chemistry of starch studied by ^{13}C high resolution solid-state NMR spectroscopy. Polymer 43:5791–5796
35. Mano JF, Koniarova D, Reis RL (2003) Thermal properties of thermoplastic starch/synthetic polymer blends with potential biomedical applicability. J Mater Sci: Mater Medicine 14: 127–135
36. Bryce DJ, Greenwood CT (1963) The thermal degradation of starch. Part III. The formation of decomposition products from starch and related materials at temperatures between 175 °C and 400 °C. Starch-Stärke 15:359–363
37. Su S, Wilkie CA (2004) The thermal degradation of nanocomposites that contain an oligomeric ammonium cation on the clay. Polym Degrad Stabil 83:347–362
38. Zheng P, Ling XK (2007) A thermal degradation mechanism of polyvinyl alcohol/silica nanocomposites. Polym Degrad Stabil 92:1061–1071
39. Liu X, Yu L, Liu H, Chen L, Li L (2008) In situ thermal decomposition of starch with constant moisture in a sealed system. Polym Degrad Stabil 93:260–262
40. Zhou XY, Jia DM, Cui YF, Xie D (2009) Kinetics analysis of thermal degradation reaction of PVA and PVA/starch blends. J Reinf Plast Compos 28:2771–2780
41. NIST Mass Spec Data Center, SE Stein (2005) "Mass Spectra" in NIST Chemistry WebBook, NIST Standard Reference Database Number 69. In: PJ Linstrom, WG Mallard (eds), National Institute of Standards and Technology, Gaithersburg, 20899. (http://webbook.nist.gov)
42. Glagovich N, (2007) Mass Spectrometry. http://www.chemistry.ccsu.edu/glagovich/teaching/316/index.html

43. Tietz M, Buettner A, Conde-Petit B (2008) Changes in structure and aroma release from starch–aroma systems upon α-amylase addition. Eur Food Res Technol 227:1439–1446
44. Tietz M, Buettner A, Conde-Petit B (2008) Interaction between starch and aroma compounds as measured by proton transfer reaction mass spectrometry (PTR-MS). Food Chem 108:1192–1199
45. Jang BN, Wilkie CA (2005) The thermal degradation of polystyrene nanocomposites. Polymer 46:2933–2942
46. Jang BN, Wilkie CA (2005) The effect of clay on the thermal degradation of polyamide 6 in polyamide 6/clay nanocomposites. Polymer 46:3264–3274